IEEE Access
Multidisciplinary | Rapid Review | Open Access Journal

Received September 14, 2020, accepted September 25, 2020, date of publication September 29, 2020,
date of current version October 9, 2020.

Digital Object Identifier 10.1109/ACCESS.2020.3027633

Digital Collaborative Development of a High Reliable Auxiliary Electric Drive System for eTransportation: From Dual Three-Phase PMSM to Control Algorithm

SHUAI HE[1,2], YAOHENG LI[1], GUANGMING ZHOU[1], JIANGTAO GAI[1], YASHAN HU[3], YONG LI[1], YING ZHANG[1], YAO CHEN[1], DERONG LUO[3], YAOJING FENG[3], AND ZHIBIN SHUAI[1,2], (Member, IEEE)

[1]Science and Technology on Vehicle Transmission Laboratory, China North Vehicle Research Institute, Beijing 100072, China
[2]State Key Laboratory of Automotive Safety and Energy, Tsinghua University, Beijing 100084, China
[3]College of Electrical and Information Engineering, Hunan University, Changsha 410082, China

Corresponding authors: Jiangtao Gai (jiangtaogai@163.com) and Zhibin Shuai (shuaizhibin@163.com)

This work was supported in part by the National Natural Science Foundation of China under Grant 51505436 and Grant 51975543, and in part by the State Key Laboratory of Automotive Safety and Energy under Project KF2018.

ABSTRACT For electrified transportation (eTransportation) systems, multi-phase motors can provide higher performance and reliability than three-phase ones, but also bring more challenges in their optimal design and control. In this article, a set of high reliable electric drive system based on dual three-phase permanent magnet synchronous motor (DTP PMSM) is developed for auxiliary systems in eTransportation field. A digital collaborative develop process is proposed with the support of multiple software tools. Design, manufacture, and bench testing stages of the DTP PMSM, the two-level six-phase inverter, and the control algorithm are efficiently incorporated. A prototype of the multi-phase electric drive system is fabricated and tested. Comparison of the simulation analysis and experimental results confirms the effectiveness of the collaborative develop progress. Control algorithms based on dual d-q model and vector space decomposition model are both verified and compared via the bench test. Operation mode switching from six-phase mode to three-phase mode is also realized with the prototype system, verifying its capability in fault-tolerant and potential in efficiency optimizing.

INDEX TERMS Dual three-phase motor, auxiliary electric drive system, transportation electrification, digital collaborative development, motor design and control.

I. INTRODUCTION

Transportation electrification is bringing a worldwide technical revolution during the past decades, benefitting from its environmental friendliness, high energy efficiency, and good propulsion performance [1], [2]. Electric transportation systems such as electric vehicles (EVs), more/all electric aircrafts and electric ships, are gaining more and more attentions from engineers and researchers all over the world [3]. In general, electric transportation systems desire that their electric drive systems satisfy the following requirements: good energy efficiency and power performance, low vibration and noise, reduced volume and weight, great robustness and fault-tolerance ability [4]. In fact, multi-phase electric drive systems, compared with classic three-phase ones, may provide a more effective solution meeting all the aforementioned challenging requirements [4], [5].

There have been various applications of multi-phase motors in the field of electrified transportation [6]. A dual three-phase motor was designed and compared with the Nissan leaf three-phase machine, and shown improved torque density and torque quality without compromising efficiency [7]. Authors in [8] combined hybrid energy storage system with dual three-phase permanent magnet synchronous motor (DTP PMSM), achieving simplified powertrain and good performance for an EV. A nine-phase machine was

The associate editor coordinating the review of this manuscript and approving it for publication was Sudhakar Babu Thanikanti.

integrated into the on-board battery charger of EVs, with a fuzzy logic controller designed for charging control [9]. Besides electric propulsion systems, the electrified auxiliary systems, such as electric actuators and electric pumps, also prefer multi-phase configurations. Six-phase motors have been widely employed by safety critical systems such as electric power steering systems (EPS) [10], [11] and electric braking systems (EBS) [12] of electrified vehicles.

Due to the application demands of multi-phase motors, there have been plentiful studies and achievements in their design, modeling and control. Among various types of multi-phase motors, a very interesting option is the dual three-phase machine consisting of two sets of three-phase windings with isolated neutral points. DTP PMSM with 24 slots have been widely studied and optimized for better torque performance and low harmonic [13], [14]. Effect of phase shift angle on radial force and vibration behavior in DTP PMSM was studied in [15]. Authors in [16] provided analytical model of N × 3-phase PMSM for control-oriented purpose. In [17], a control algorithm was specially designed to drive a dual three-phase induction motor with a five-leg inverter. High quality current control [18], [19] and fault-tolerant control [20], [21] are also research hotspots of DTP motors.

More phases bring more novel configurations and design innovations as well. In a six-phase hybrid-excitation motor, three phases were used as excitation winding while the other three phases worked as armature winding [22]. In [23], novel toroidal windings were proposed for a six-phase direct-drive PMSM. In [24], windings of two six-phase induction motors were connected in series, and independently controlled from a single six-phase inverter. A six-phase transverse flux tubular permanent magnet linear motor was designed with a fault-tolerant control strategy in [25]. Authors in [26] optimized the torque profile of a six-phase PMSM for a direct-drive EV with supervised machine learning. In [27], multi-level inverter was optimally designed with two sets of three-phase windings for better fault-tolerant and reduced torque ripple of an induction motor.

As previously reviewed, multi-phase configurations can provide more optimizing potentials and flexibility to electric-drive systems. However, there are also some challenges in the development process of multi-phase systems for electrified transportation. Transportation facilities such as electrified vehicles are systems with multiple requirements, constraints, and trade-offs. Most of existing studies mainly focus on individual research point of multi-phase systems, such as motor design, inverter configuration, or control algorithm. Collaborative development of the whole multi-phase systems is urgently desired for their application in eTransportation. The multi-phase motor, the inverter, and the control algorithm should be synergistically researched and developed, to achieve comprehensive optimum scheme of the whole system, and meet the rigorous requirements in power, efficiency, weight, volume, and reliability.

Facing those aforementioned challenges, some work has been carried out in this article. The main contributions of this work are twofold. First, a multi-software based digital collaborative development process is proposed and practiced in this work, achieving higher development efficiency and optimized performance of the multi-phase electric drive system. Design, manufacture and validation of the DTP PMSM, the six-phase two-level inverter, and the control algorithm are efficiently coordinated and iterated in the design loop. Second, two kinds of control algorithms for the DTP PMSM are designed with simulation, applied to actual system, and compared via experiments. Torque ripple suppression and fault-tolerant capabilities of the whole system have been adequately validated via bench tests.

The remaining sections of this article are organized as follows. In Section II, the design problem of the multi-phase electric drive system is formulated, and the multi-software based digital collaborative development process is introduced. In Section III, the design, optimization and simulation analysis of the DTP PMSM is elaborated. Section IV presents the design of a six-phase two level inverter as the controller of the DTP PMSM. In Section V, control-oriented models of the DTP PMSM are built, and control algorithm is developed. Section VI accomplishes experimental validation of the motor prototype and the controller, and gives some discussions. Conclusions of this article are drawn in Section VII.

II. DIGITAL COLLABORATIVE DEVELOPMENT PROCESS OF THE AUXILIARY ELECTRIC DRIVE SYSTEM

A. PROBLEM FORMULATION

Oil pumps are key auxiliary components in vehicle powertrain systems, and electric-drive oil pumps are especially meaningful for hybrid powertrains [28], [29]. In this work, a high reliable 6kW DTP PMSM system is developed for oil pumps of electrified vehicles, and also can be applied to auxiliary systems of other electrified transportation facilities.

It should be noted that, limited by the on-board power distribution scheme, a DC bus voltage scheme is determined as 260V-280V which is also consistent with other auxiliary voltage systems of aviation and marine transportation. Primary requirements of the system are listed in Table 1.

TABLE 1. Primary requirements of the auxiliary system.

Parameter	Value
Rated power	6 kW
Rated speed	3000 rpm
Cooling method	Natural cooling
Speed sensor	Resolver

For the DTP PMSM system, two aspects should be taken into account: Firstly, a high power-density motor with good performance should be designed with multi-factor optimizing. The slot-pole combination and the rotor magnetic circuit should be optimized so as to reduce the cogging torque and leakage inductance of the motor, and improve the torque output and efficiency at the same time. Secondly, a high efficiency motor controller is expected to maximize the

efficiency of the motor, make full use of DC bus voltage, enhance the system response, and guarantee the stability and robustness of the whole system. The design process should be rapidly iterated to improve the development efficiency.

Therefore, strong requirements for the collaborative design process of the motor and controller have been put forward, along with the development of high-performance auxiliary electric drive system.

B. DIGITAL COLLABORATIVE DEVELOPMENT PROCESS OF THE ELECTRIC DRIVE SYSTEM

In order to satisfy the aforementioned requirements, an efficient development method needs to be used. Multiple engineering tools, such as EDA and CAD software, have evolved in the last decades and different solutions for electrical, mechanical and software engineering enable a high efficiency digital design process of the electric drive system [30]–[32]. On the one hand, the digital design process has been conducive to shorten the development cycle and lower the economic cost, because requirements from one phase can be directly taken into account in other phases, and meanwhile, independent work can be done parallelly. On the other hand, product data management (PDM) has been widely employed in the industry, and data exchanging between engineering tools and the database is more convenient in this way. Fig.1 shows the main engineering tools helping enhance the development efficiency.

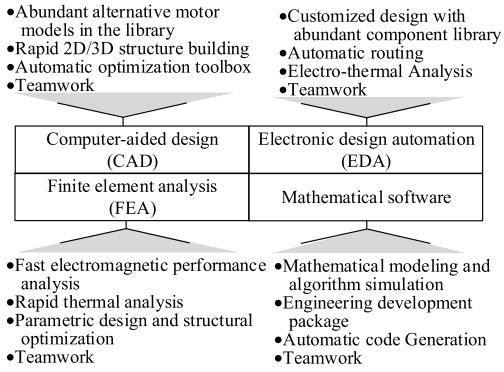

FIGURE 1. Efficient development tools of engineering software.

The digital development process with multi-software collaboration is depicted in Fig. 2. According to demands, design tasks can be decomposed into different sub processes including motor design, controller hardware design, and software design. To better understand data exchanging between different phases, the detailed processes have been summarized in Fig.3.

For motor design, multi parameters optimization is essential to improve motor performance. With the help of motor design software, a preliminary scheme can be directly selected from the abundant alternative motor libraries including brushless permanent magnet motors (BPM), induction machines (IM) and so on, which has a low demand of engineering experience for designers. And finite element analysis (FEA) can be utilized to carry out the simulation results of motor performance for parameters optimization design such as winding cogging scheme and magnetic circuit structure. Due to switching frequency limitation and dead-time increasing the harmonic component in output voltage, it is necessary to consider the reduction of high frequency loss in motor design. The influence of modulation voltage utilization on the motor should also be considered. The detailed design and optimization results will be introduced in Section III.

In hardware design, constraint parameters including voltage and current level of each phase and DC bus are obtained from motor FEA results. To improve efficiency of development, EDA software can be used for circuit design and simulation, at the same time for electro-thermal analysis. Combined with the control algorithm suppressing harmonics, the value of the support capacitor can be reduced in the design. Moreover, by adopting automatic coding tools, the control algorithm can be easily converted from simulation algorithm to embedded code, which is much more efficient than conventional handwriting code.

During control software design, the motor parameters, such as inductance and permanent flux, can be obtained from the FEA results, and after that a high-precision mathematical model of the motor can be built for the model in the loop (MIL) analysis. In addition, the control algorithm can be optimized through collaborative development. For example, the copper loss and iron loss at different speeds calculated by FEA can be utilized to improve the control algorithm based on the minimum energy loss. For high performance control, the time delay and dead-time of inverter should be taken into account as well.

In summary, developing process based on multi-software digital collaborative design integrates the advantages of various software to improve development efficiency and flexibility. It should be pointed out that the design scheme will be optimized according to the prototype test in the form of correction factor.

III. OPTIMAL DESIGN OF THE DUAL THREE-PHASE PMSM

A. MAIN PARAMETERS DESIGN OF THE DTP PMSM

The DTP PMSM involves in two sets of Y-type three-phase stator windings with separated neutral points. Two sets of stator windings that indicated by (A, B, C) and (X, Y, Z) lay in the stator but not fracture with each other, as shown in Fig. 4. There are two kinds of winding topologies in common use: one is that the two sets of windings are completely coincident in electrical angle, namely, the windings are diverted by 0 electrical degrees, and the other is that the windings are spatially shifted by 30 electrical degrees. For the latter winding structure, due to the sixth harmonic torque generated by the two sets of windings is equal with 180° phase difference, the lowest order of the torque ripple is 12^{th}. Whereas fault tolerance and torque ripple should be considered, the scheme

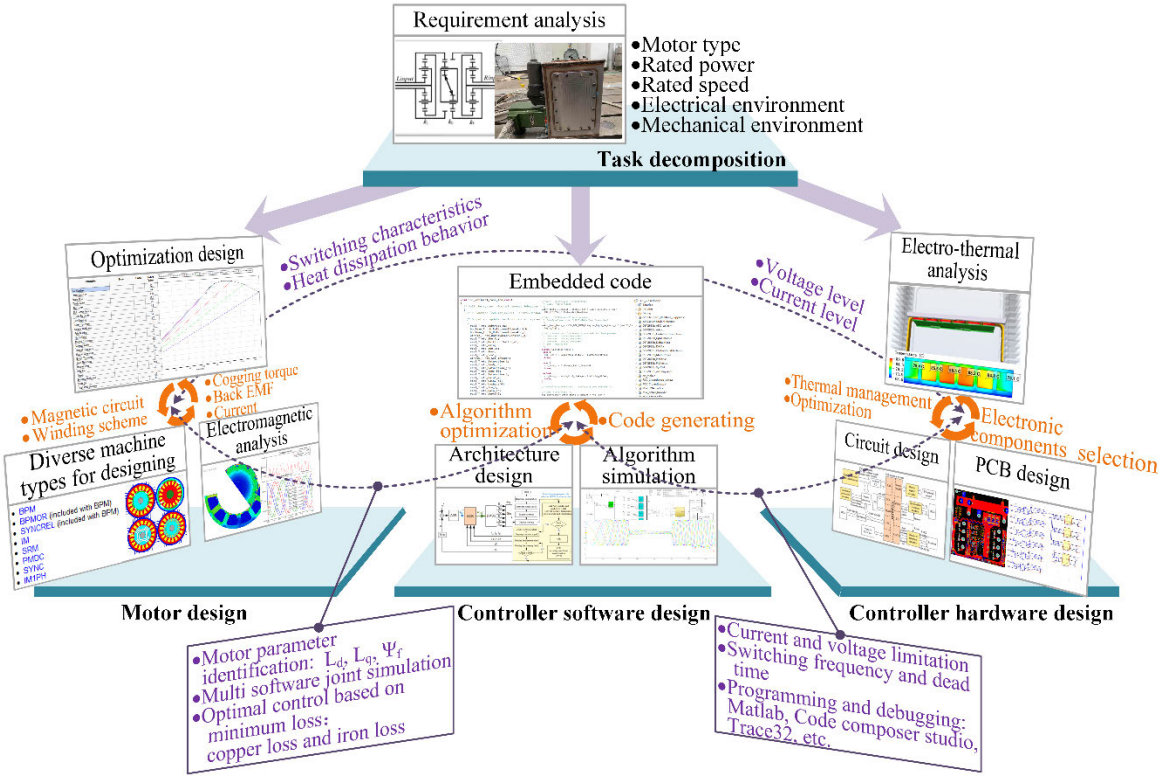

FIGURE 2. Detailed digital collaborative development process for an auxiliary electric drive system.

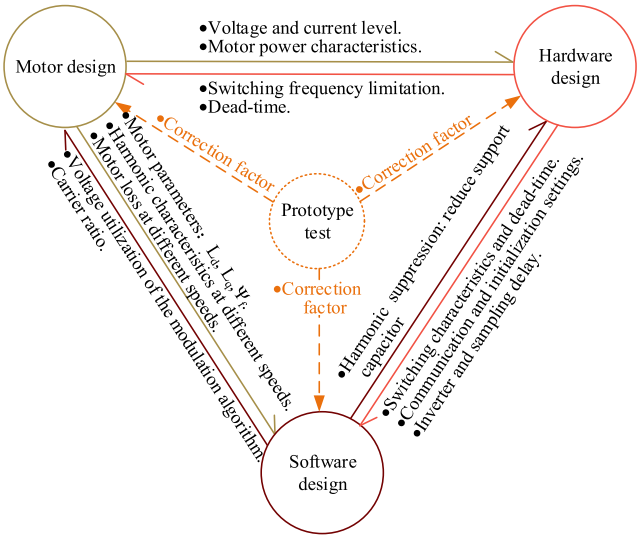

FIGURE 3. Data exchanging between multi software.

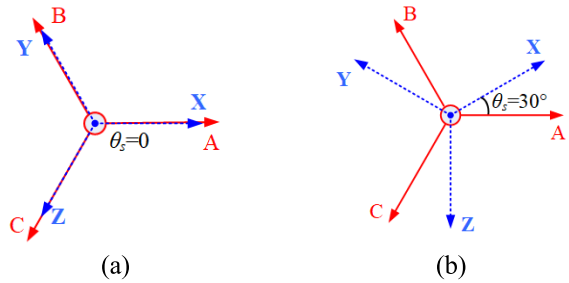

FIGURE 4. Two diagrams for DTP PMSM stator winding structure within separated neutral points. (a) Two sets of windings spatially shifted by 0°. (b) Two sets of windings spatially shifted by 30°.

with winding shifted by 30° shown in Fig. 4 (b) is employed in this article.

1) OPTIMIZATION OF THE SLOT-POLE COMBINATION

Owing to the influence of the controller switch frequency range on the system performance and hardware cost, the motor polar numbers should be considered first. In the following design, the schemes of 6,8,10 poles integral and fractional slot winding are compared.

The three schemes mentioned above can be arranged in dual-three phase stator windings with conventional integer slot scheme. The pole distance (number of slots per pole) is set to 6, and the pole slot matching schemes are respectively 6-pole/36-slot, 8-pole/48-slot and 10-pole/60-slot with the coil pitch being 5. Under the condition that other parameters and electromagnetic load of the motor are the same, the cogging torque waves for the three schemes in the range of 12 mechanical degrees at the rated speed is illustrated in Fig. 5.

The cogging torque of electrical machine with integral slot winding is large, which can be reduced by fractional slot

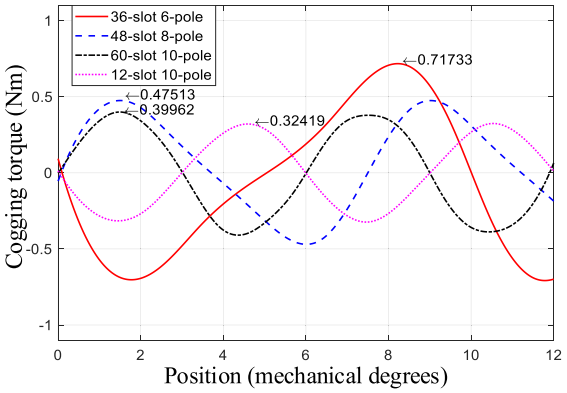

FIGURE 5. The comparison of cogging torque for different pole slot matching schemes with integral slot.

winding [13], [14], as shown in Fig.5. After FEA, 10-pole/12-slot fractional-slot double-layer winding scheme is adopted, by which the peak value of cogging torque is less than 0.45N·m, and the distortion rate of line back EMF waveform is small.

2) OPTIMAL DESIGN OF ROTOR MAGNETIC CIRCUIT

The rotor permanent magnet of DTP PMSM is usually fixed in two ways: surface mounted pole structure and interior pole structure. The surface mounted permanent magnet is located on the outer surface of the rotor core. In order to avoid the permanent magnet being thrown out during the rotation of the motor, the outer surface of the permanent magnet is usually covered with a non-magnetic sleeve or tied with a fiberglass tape to protect it. Due to the poor mechanical performance of the surface mounted structure, which is not suitable for high-speed motors, the interior structure is adopted as shown in Fig.6(a). Since the permanent magnet size and the pole arc coefficient are constant, the measure of magnetic isolation becomes the decisive factor of motor performance, containing the rib (the rib between adjacent magnet poles) and the bridge (the bridge between outer web corners and rotor surface).

The optimal design is carried out through changing the bridge thickness since the rib thickness mainly affects mechanical strength rather than electromagnetic performance of the motor. The bridge thickness varies from 1.0 mm to 2.0 mm in a scale of 0.1 mm, and Fig.6(b) presents the electromagnetic performance obtained by FEA. For the motor, the cogging torque and airgap flux density shall be small, and the back EMF shall be close to and slightly smaller than the power supply voltage. Besides, in order to improve sufficient mechanical strength, the bridge thickness shall not be too small.

Considering comprehensively, we believed that the scheme with 1.5 mm bridge thickness was the best option. The parameters of the DTP PMSM are determined as shown in Table 2.

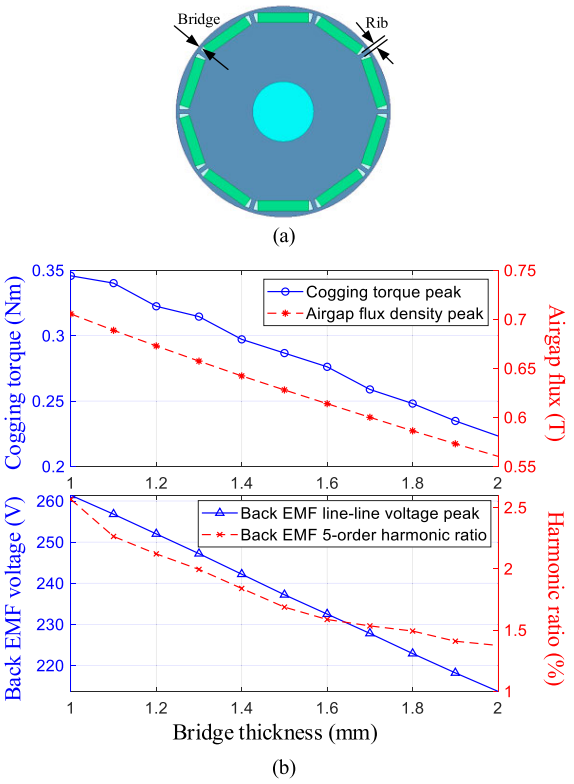

FIGURE 6. Rotor magnetic circuit structure and FEA results for electromagnetic performance. (a) 10-pole interior radial rotor magnetic circuit structure. (b) Comparison of electromagnetic performance under 1 mm to 2 mm bridge width.

TABLE 2. Main design parameters of DTP PMSM.

Parameter	Value
Stator lamination diameter (mm)	174
Stator core length (mm)	100
Pole pairs	5
Slot number	12
Stacking factor of stator	0.95
Type of stator winding	Double-layer winding
Airgap width (mm)	1.0
Bridge thickness (mm)	1.5
Rib thickness (mm)	2.0
Silicon steel sheet type of stator	M27 36F180
Silicon steel sheet type of rotor	M27 36F180
Permanent magnet sheet type	Samarium Cobalt S28
Permanent magnet sheet type	Samarium Cobalt S28

B. ELECTROMAGNETIC SIMULATION AND ANALYSIS OF THE OPTIMAL SCHEME

According to the proposed optimal design scheme of the DTP PMSM, the performance was evaluated under the no-load and rated operation conditions in terms of the flux density, back EMF, current and torque. The results were represented in Figs.7(a)-(e).

The magnetic field distribution in the motor shows that the flux density of stator teeth is under 1.8 T while the flux

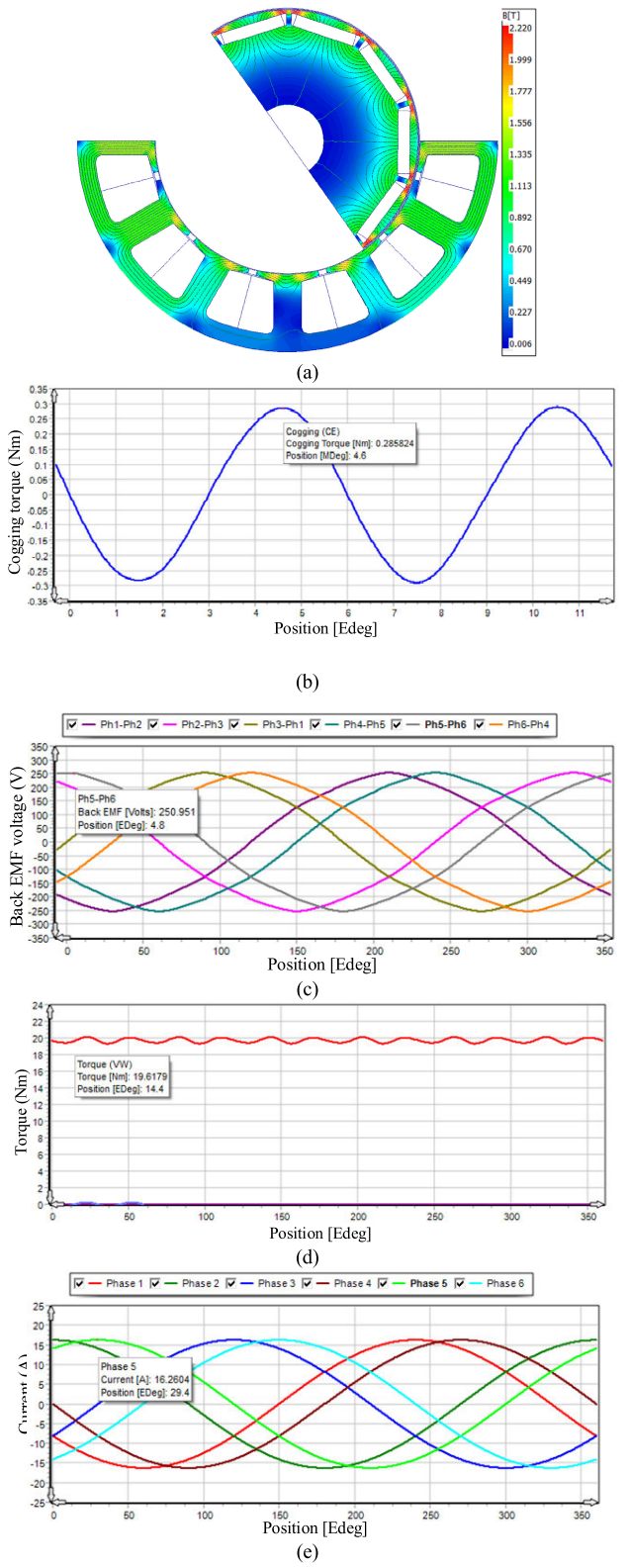

FIGURE 7. Performances of the DTP PMSM. (a) The magnetic field distribution in the motor with no load. (b) Cogging torque of the motor. (c) Back EMF at the rated speed (3000 rpm) (Ph1-Ph2 represents line-line back EMF voltage U_{XY}). (d) Torque at the rated load (19.1 Nm). (e) Phase current under rated operating condition (phase 1 to phase 6 represent phases *A*, *B*, *C*, *X*, *Y*, *Z* respectively).

density of rotor bridge is locally over 2.0 T with no load, which is beneficial for the flux to go into the stator core from the teeth after passing through the air gap. Therefore, it can be considered that, theoretically, the magnetic circuit design of the motor is reasonable and provides good material utilization.

The peak value of no-load cogging torque is about 0.29 Nm, accounting for 1.52% of the rated torque (19.1 Nm), which is quite small. At the rated speed 3000 rpm, the line-line back EMF waveform is sinusoidal and its RMS is 178 V.

According to FFT, fundamental back EMF amplitude is 245 V with THD under 1.80%. Taking the existence of friction resistance and stray loss into account, the electromagnetic torque at the rated load is 19.6 Nm slightly higher than the rated value, and the steady-state current is 11.5 A, having sinusoidal waveform and low harmonic components. Hence, from a mathematical point of view, the design of winding meets the requirement under either set of conditions.

IV. DESIGN OF THE SIX-PHASE TWO-LEVEL INVERTER FOR THE DTP PMSM SYSTEM

A. TECHNICAL SCHEME OF THE CONTROL SYSTEM

Based on the demand for auxiliary electric drive system, the following general technical solutions are adopted. The DC bus voltage provided by the on-board battery is inputted into the driving circuit after filtering by support capacitors. The DTP PMSM is fed by a six-phase two-level voltage source inverter (2L-VSI). The digital signal processing (DSP) chip is used to generate PWM signals and drive 2L-VSI to output appropriate AC voltage. The DTP PMSM operates in the control pattern of rotational speed, and is able to switch over between single three-phase (STP mode) and double three-phase operation modes (DTP mode) automatically and smoothly, so as to deal with the failure of a certain phase and remain running for a short time. Upon over-current fault or over-voltage fault occurring, the control system can cut off the AC voltage instantly to stop the motor.

Six-phase VSI is deemed to combine two three-phase VSIs, hence two three-phase H-bridge intelligent power modules (IPMs) can be utilized to form the driving circuit. IPMs, integrating IGBTs and circuit of logic, control, monitoring and protection, have the advantages of compact structure and high reliability. Moreover, owing to the low power and load current of oil pump motor, the scheme by using IPMs is suitable enough for design requirements.

The main controller chip is a 32-bit single-precision floating-point DSP, TMS320F28335, produced by Texas Instruments (TI) (Dallas, TX, USA). This processor is used to start the DTP PMSM; control the speed of the motor; switch over among two operation modes; provide protection for over-current, over-voltage and overheat of the motor and the controller; and also provide data communication interface of RS485 and CAN.

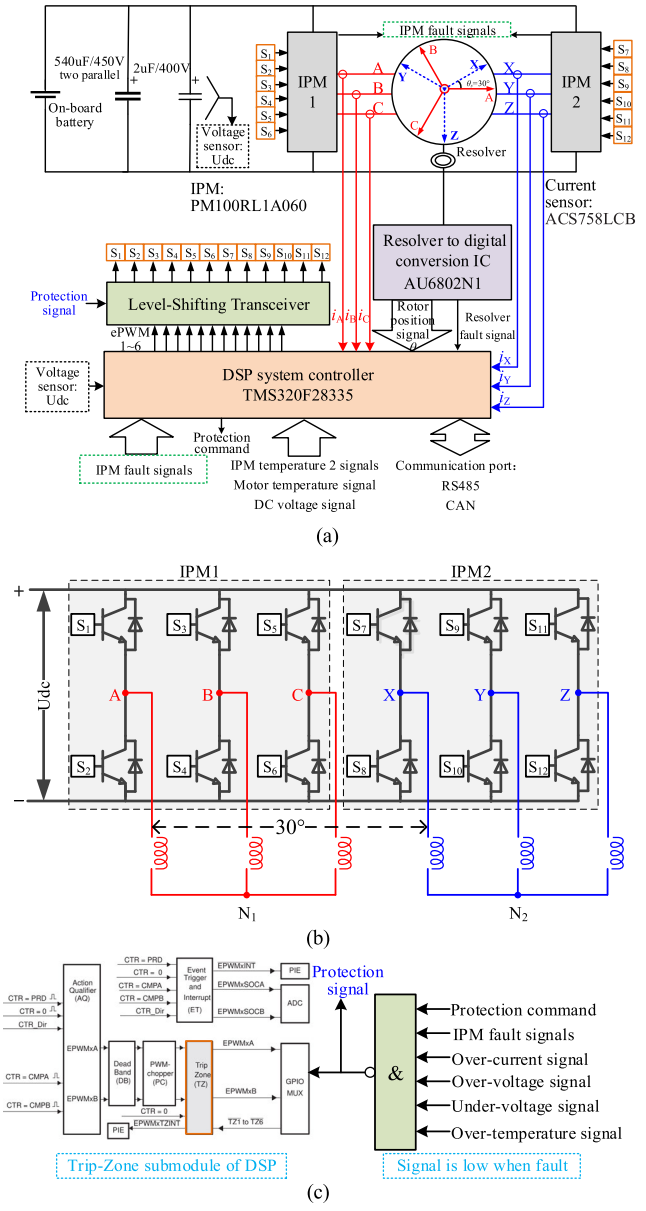

FIGURE 8. The schematic diagram of main power circuit. (a) Main power circuit. (b) The internal circuit of six-phase VSI with two IPMs in parallel. (c) Protection circuitry scheme.

B. HARDWARE DESIGN OF THE HIGH-VOLTAGE MAIN POWER CIRCUIT

As shown in Fig. 8(a), the main power loop for the DTP PMSM is composed of the on-board battery; large DC filter capacitors (DC-link support capacitors); two IPMs; sampling of current, voltage, temperature and speed signals; communication interface; and system controller.

The basic working process of the main power circuit is as follows: the on-board battery provides 260-280V DC voltage, and through 540μF/450V capacitors (two 270μF/450V capacitors in parallel) and a 2μF/400V non-inductive absorption (high-frequency) capacitor, the DC bus voltage becomes relatively stable and the ripple is greatly improved. And then, the DC bus voltage is input into two IPMs. After modulation with control algorithms, the six-phase (*ABCXYZ*) high voltage is generated by IPMs, which is directly applied to two sets of three-phase windings of the DTP PMSM. The internal circuit of IPMs is illustrated in Fig. 8 (b). In addition to realizing the function of the DC/AC inverter, the IPMs can send the fault signals to the DSP as well, which is vital for protecting the equipment.

The DSP controller samples real-time signals of DC bus voltage, stator current, and rotor position and speed, and then sends 12-channel PWM signals generated by closed-loop control algorithm to drive the IPMs. Besides, the controller can realize software protection by analyzing the fault signal from peripherals, and it can send out a protection signal in the case of faults. The level-shifting transceiver not only translates PWM signals from 3.3V to 5V for asynchronous communication between data buses, but also disables PWM signals translation when receiving DSP's protection signal, so as to respond to software protection command.

C. HARDWARE DESIGN OF THE DIGITAL CIRCUIT

The hardware part of the DTP PMSM controller, shown in Fig.9, includes the DSP minimum system, power supply circuitry, optocoupler isolation circuitry, signals detection and conditioning circuitry, resolver interface circuitry, hardware protection circuitry, and communication circuitry.

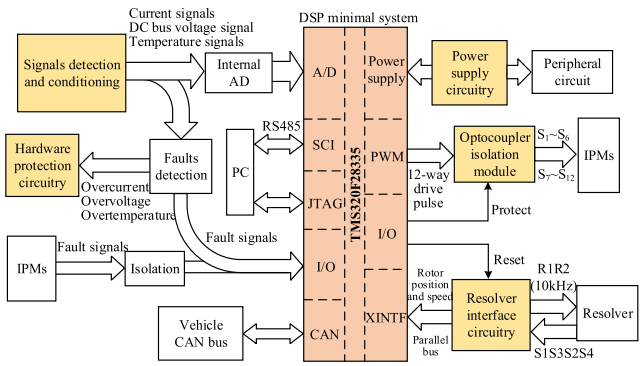

FIGURE 9. Schematic diagram of the controller hardware.

The minimum system of the DSP, TMS320F28335, consists of the chip power supply (3.3 V, 1.8 V), 30 MHz external crystal oscillator (the maximum working frequency of the chip is 150 MHz through PLL frequency modulation), 14-pin JTAG interface for program debugging, as well as requisite bias resistors and bypass capacitors.

Power supply circuitry is DC/DC conversion circuit, providing stable voltage source for the DSP and peripheral circuits. Optocoupler isolation module is an essential part of IPMs drive circuit, isolating high voltage from low voltage. The analog signals from sensors before being sent to AD module will be filtered and denoised by signal detection and conditioning circuitry so as to improve the sampling accuracy. Furthermore, resolver as a position sensor needs the resolver interface circuitry, including the exciting signal circuit and

resolver/digital converter (RDC), to detect the rotor position and speed information, and output digital signals of rotor position and speed to external interface (XINTF) data lines of DSP through parallel ports.

Hardware protection circuitry automates protecting for over-current, DC bus over-voltage or under-voltage, and over-temperature realized by voltage comparator circuit, which is a supplement for software protection. As shown in Fig.8(c), protection signal is generated after fault signals and protection command passing through a NAND gate. Trip-zone (TZ) submodule of DSP connecting to protection signal is programmed to respond when faults occur. For example, upon over-current detected, protection signal will be forced to shift level ignoring software command, and TZ will disable PWM signals output from DSP, and meanwhile, the level-shifting transceiver in Fig.8(a) will be disabled as well. Other fault signals are processed in the same way.

V. CONTORL SOFTWARE DESIGN OF THE DTP PMSM

A. CONTROL-ORIENTED MODELS OF THE DTP PMSM

Two analysis methods for the DTP PMSM in different coordinate systems are introduced in this section, corresponding to different mathematical models: dual d-q transformation model and vector space decomposition (VSD) model. The dual d-q transformation regards each set of three-phase windings as a basic unit, and applies the conventional three-phase motor modeling method to each set of three-phase windings separately, which can be regarded as two three-phase motors with coupling relationship. According to VSD method, the overall machine model, such as fundamental components, harmonic components and zero sequence components, is transformed and decomposed into three decoupled subspaces, corresponding to electromechanical energy conversion and harmonic loss respectively [18], [24].

In the dual d-q model, six variables of the DTP PMSM are transformed into two sets of reference variables [33], which can be expressed in stationary frame as d_1-q_1 components and d_2-q_2 components respectively by:

$$\begin{aligned} \begin{bmatrix} d_1 & q_1 & d_2 & q_2 \end{bmatrix}^T &= P_{6s/2qd} \cdot \begin{bmatrix} A & B & C & X & Y & Z \end{bmatrix}^T \\ P_{6s/2dq} &= \begin{bmatrix} P_1 & O \\ O & P_2 \end{bmatrix} \end{aligned} \tag{1}$$

where:

$$P_1 = \frac{2}{3}\begin{bmatrix} cos\,\theta & cos\left(\theta - \frac{2\pi}{3}\right) & cos\left(\theta + \frac{2\pi}{3}\right) \\ -sin\theta & -sin\left(\theta - \frac{2\pi}{3}\right) & -sin\left(\theta + \frac{2\pi}{3}\right) \end{bmatrix}$$

$$P_2 = \frac{2}{3}\begin{bmatrix} cos\left(\theta - \frac{\pi}{6}\right) & cos\left(\theta - \frac{5\pi}{6}\right) & cos\left(\theta + \frac{\pi}{2}\right) \\ -sin\left(\theta - \frac{\pi}{6}\right) & -sin\left(\theta - \frac{5\pi}{6}\right) & -sin\left(\theta + \frac{\pi}{2}\right) \end{bmatrix}$$

θ is the electrical angle between d_1 axis and phase A axis, O is a zero matrix of 2 rows × 3 columns.

Stator voltage equation and flux equation in the dual d-q model are expressed respectively as follows:

$$\begin{aligned} \begin{bmatrix} u_{d1} \\ u_{q1} \\ u_{d2} \\ u_{q2} \end{bmatrix} &= \begin{bmatrix} R_s & 0 & 0 & 0 \\ 0 & R_s & 0 & 0 \\ 0 & 0 & R_s & 0 \\ 0 & 0 & 0 & R_s \end{bmatrix} \begin{bmatrix} i_{d1} \\ i_{q1} \\ i_{d2} \\ i_{q2} \end{bmatrix} \\ &\quad + \frac{d}{dt}\begin{bmatrix} \psi_{d1} \\ \psi_{q1} \\ \psi_{d2} \\ \psi_{q2} \end{bmatrix} + \omega \begin{bmatrix} -\psi_{q1} \\ \psi_{d1} \\ -\psi_{q2} \\ \psi_{d2} \end{bmatrix} \end{aligned} \tag{2}$$

$$\begin{bmatrix} \psi_{d1} \\ \psi_{q1} \\ \psi_{d2} \\ \psi_{q2} \end{bmatrix} = \begin{bmatrix} L_d & 0 & L_{dd} & 0 \\ 0 & L_q & 0 & L_{qq} \\ L_{dd} & 0 & L_d & 0 \\ 0 & L_{qq} & 0 & L_q \end{bmatrix} \begin{bmatrix} i_{d1} \\ i_{q1} \\ i_{d2} \\ i_{q2} \end{bmatrix} + \begin{bmatrix} 1 \\ 0 \\ 1 \\ 0 \end{bmatrix} \psi_{\mathrm{fd}} \tag{3}$$

where:

$$\begin{aligned} L_d &= 3/2L_{aad} + L_{aal}, \\ L_q &= 3/2L_{aaq} + L_{aal}, \\ L_{dd} &= 3/2L_{aad}, \\ L_{qq} &= 3/2L_{aaq}, \end{aligned}$$

R_s, L_{aad}, L_{aaq}, and L_{aal} are the stator resistance and inductances. ω is the electric angular frequency. ψ_{fd} is amplitude of rotor flux.

Electromagnetic torque equation of the motor with pole pairs p_0 in the dual d-q model can be obtained:

$$T_e = 3/2p_0\left(i_{q1}\psi_{d1} - i_{d1}\psi_{q1} + i_{q2}\psi_{d2} - i_{d2}\psi_{q2}\right) \tag{4}$$

The electromagnetic torque equation indicates that the total torque of the DTP PMSM is a superposition of the torque generated by two sets of windings. Due to mutual inductance between the two sets of windings, this kind of torque superposition is not linear, nevertheless, it is obvious that the DTP PMSM has larger torque peak than the three-phase motor, under the same current limits and electrical parameters of d and q axes.

The relationship between the VSD variables and the motor variables is given in the following formula [34]:

$$\begin{aligned} \begin{bmatrix} d & q & z_1 & z_2 \end{bmatrix}^T &= T_{6s/dqz1z2} \cdot \begin{bmatrix} A & B & C & X & Y & Z \end{bmatrix}^T \\ T_{6s/\mathrm{dqz1z2}} &= 1/3\begin{bmatrix} T_1 & T_2 \end{bmatrix} \end{aligned} \tag{5}$$

where:

$$T_1 = \begin{bmatrix} cos\theta & cos\left(\theta - \frac{2\pi}{3}\right) & cos\left(\theta + \frac{2\pi}{3}\right) \\ -sin\theta & -sin\left(\theta - \frac{2\pi}{3}\right) & -sin\left(\theta + \frac{2\pi}{3}\right) \\ 1 & -\frac{1}{2} & -\frac{1}{2} \\ 0 & -\frac{\sqrt{3}}{2} & \frac{\sqrt{3}}{2} \end{bmatrix}$$

$$T_2 = \begin{bmatrix} cos\left(\theta - \frac{\pi}{6}\right) & cos\left(\theta - \frac{5\pi}{6}\right) & cos\left(\theta + \frac{\pi}{2}\right) \\ -sin\left(\theta - \frac{\pi}{6}\right) & -sin\left(\theta - \frac{5\pi}{6}\right) & -sin\left(\theta + \frac{\pi}{2}\right) \\ -\frac{\sqrt{3}}{2} & \frac{\sqrt{3}}{2} & 0 \\ \frac{1}{2} & \frac{1}{2} & -1 \end{bmatrix}$$

Stator voltage equation and flux equation in VSD model are expressed respectively as follows:

$$\begin{bmatrix} u_d \\ u_q \\ u_{z1} \\ u_{z2} \end{bmatrix} = \begin{bmatrix} R_s & 0 & 0 & 0 \\ 0 & R_s & 0 & 0 \\ 0 & 0 & R_s & 0 \\ 0 & 0 & 0 & R_s \end{bmatrix} \begin{bmatrix} i_d \\ i_q \\ i_{z1} \\ i_{z2} \end{bmatrix} + \frac{d}{dt} \begin{bmatrix} \psi_d \\ \psi_q \\ \psi_{z1} \\ \psi_{z2} \end{bmatrix} + \omega \begin{bmatrix} -\psi_q \\ \psi_d \\ 0 \\ 0 \end{bmatrix} \tag{6}$$

$$\begin{bmatrix} \psi_d \\ \psi_q \\ \psi_{z1} \\ \psi_{z2} \end{bmatrix} = \begin{bmatrix} L_D & 0 & 0 & 0 \\ 0 & L_Q & 0 & 0 \\ 0 & 0 & L_Z & 0 \\ 0 & 0 & 0 & L_Z \end{bmatrix} \begin{bmatrix} i_d \\ i_q \\ i_{z1} \\ i_{z2} \end{bmatrix} + \begin{bmatrix} 1 \\ 0 \\ 0 \\ 0 \end{bmatrix} \psi_{fd} \tag{7}$$

where

$$\begin{aligned} L_D &= 3L_{aad} + L_{aal}, \\ L_Q &= 3L_{aaq} + L_{aal}, \\ L_Z &= L_{aal}. \end{aligned}$$

Electromagnetic torque equation of the motor with pole pairs p_0 in VSD model can be obtained:

$$T_e = 3p_0\left(i_q\psi_d - i_d\psi_q\right) \tag{8}$$

In fact, the control method with dual d-q control is very similar to VSD method. The former is easy to be understood and realized, but with more complex voltage decoupling problems. Although the latter decouples the fundamental component and harmonics completely, the physical meaning of variables in VSD control is not so clear compared with the double d-q control. In this article, both of the above two mathematical models are used for control algorithm design: VSD model for steady-state control and double d-q model for fault-tolerant control.

For STP mode, only one set of three-phase windings is working under fault-tolerant control. When phase windings XYZ are cut off, for instance, $u_{d2} = 0$ and $u_{q2} = 0$ in (2), which is exactly the same as the voltage equation of three-phase motor. As is shown in (1), transformation matrix of dual-three phase motor can be directly transformed into that of three-phase motor without extra computation in STP mode. Therefore, the dual d-q model instead of VSD model will be used for further STP algorithm design.

B. CONTROL ALGORITHM DESIGN OF THE DTP PMSM

The control algorithm of the DTP PMSM controller is developed by model-based design (MBD) method in MATLAB/Simulink (MathWorks Corp., USA), and the embedded source code is generated by Simulink Coder toolbox. With this rapid development method, the initialization of hardware and software is automatically completed by Simulink without manual setup, and the main control program is executed in enhanced PWM (ePWM) interrupt of DSP. The control software consists of the following five functional modules: closed-loop control algorithm, operational status display, AD sampling processing, communication module and fault status monitoring.

Field orientation vector control (FOC) is adopted in the closed-loop speed-regulating strategy to control the DTP PMSM to start and reach the target speed. Whereas the operating speed of the oil pump is under the motor rated speed, the flux-weakening control is not involved here. Through orienting the flux on the d-axis and setting d-axis reference current to 0, (4) and (8) can be written respectively as

$$T_e = 3/2p_0\left(i_{q1}\psi_{d1} + i_{q2}\psi_{d2}\right) \tag{9}$$

$$T_e = 3p_0 i_q \psi_d \tag{10}$$

Thus, FOC can control the electromagnetic torque output of the motor by adjusting the q-axis current, in order to minimize the dependence of control system on motor parameters. Fig.10(a) is a principle block diagram of the operation control strategy, which adopts double closed-loop vector control of speed and current.

The reference value of q-axis current (i_q^*) is calculated by the automatic speed regulator (ASR) taking the speed error through comparing the given value (n^*) with the sampling value (n) as the input. Detecting the current from the six-phase windings of the motor and using the coordinate transformation, according to (1) and (5), the current used by the regulator are obtained, as shown in Figs. 10 (b) and (c). These values are compared with the given values, and the voltage reference values of each axis (u_{ref}) are calculated by the respective PI regulators. In Fig. 10 (b), the strategy based on the double d-q model treats the DTP PMSM as two three-phase motors, and sets d-axis current reference (i_{d1}^*, i_{d2}^*) value to zero while q-axis current reference (i_q^*) value given by ASR. In Fig.10(c), the harmonic current in the $z1$-$z2$ subspace (i_{z1}, i_{z2}) is obtained by VSD, despite independent of the energy conversion of the motor, and will contribute to the copper loss, therefore, the reference value of the harmonic current (i_{z1}^*, i_{z2}^*) is given to zero, while the current of the d-q subspace is the same as the former method.

The saturation algorithm of the inverter current and voltage is designed. Reference values of d and q axis current (or voltages) given by ASR (or ACR) are q_{ref} and d_{ref}, and the output value of the saturation algorithm q^* and d^* can be calculated by

$$\begin{cases} q^* = q_{\text{ref}} \\ d^* = d_{\text{ref}}, \end{cases} \quad DQ_{\text{ref}} < DQ_{\text{limit}}$$

$$\begin{cases} q^* = \dfrac{q_{\text{ref}}}{DQ_{\text{ref}}} DQ_{\text{limit}} \\ d^* = \dfrac{d_{\text{ref}}}{DQ_{\text{ref}}} DQ_{\text{limit}}, \end{cases} \quad DQ_{\text{ref}} \geq DQ_{\text{limit}} \tag{11}$$

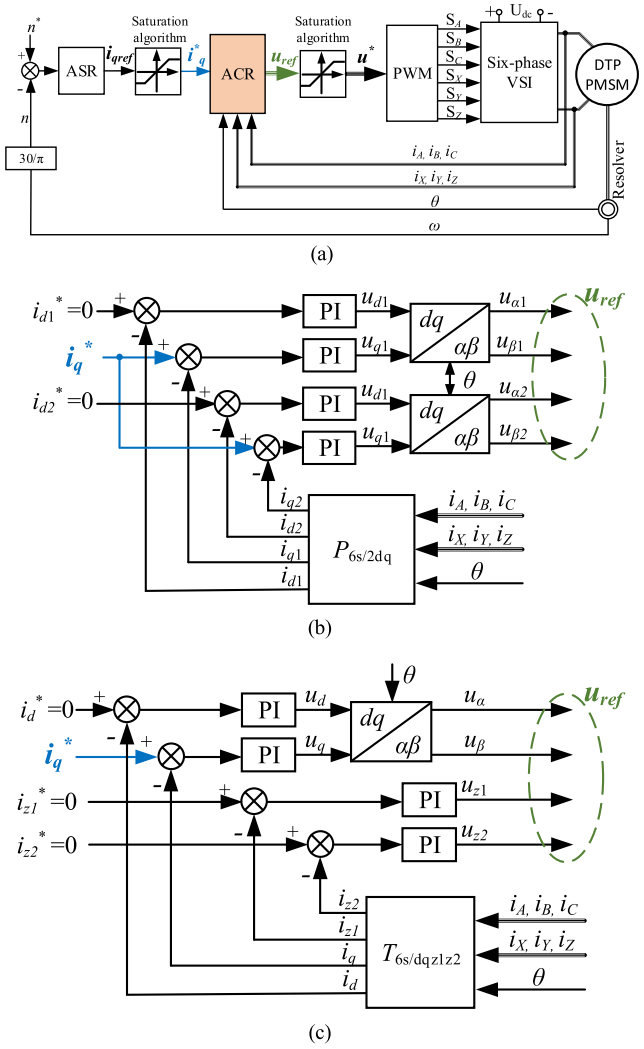

FIGURE 10. Diagram control strategy of the DTP PMSM through FOC. (a) Block diagram of the operation double loop control strategy. (b) ACR based on the dual *d-q* model. (c) ACR based on VSD.

where

$$DQ_{\text{ref}} = \sqrt{q_{\text{ref}}^2 + d_{\text{ref}}^2}$$

and DQ_{limit} is the maximum magnitude of the stator phase current (or voltage) that the inverter can supply to the motor.

Finally, by applying SVPWM, the converted PWM drive pulse (S_A-S_Z) is inputted into the six-phase VSI to generate six-phase voltage driving the motor to achieve control of the DTP PMSM.

A flowchart for control software is shown in Fig. 11. After hardware initialization and software initialization in order, the software enables interrupt and enters the circular waiting. When ePWM interrupt set as the main control program entry point occurs, the program enters the interrupt subprogram. First, the current, voltage, temperature and rotor position and speed values in real-time are obtained by AD sampling processing and XINTF to determine whether faults (such as over-current, over-voltage, over temperature and other faults)

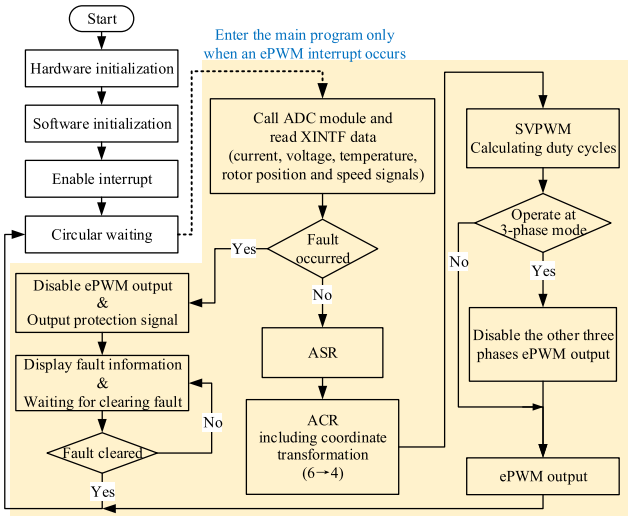

FIGURE 11. Software flowchart and main program block diagram.

have occurred. The software protection program will be executed if faults occur, sending out protection directive signal to close PWM signals output, and the corresponding fault information will be displayed by fault status monitoring module. Only after troubleshooting can the control program continue. When no fault occurs, the PWM signals of each phase is generated according to the control strategies in Figs.10(b)-(c), output through ePWM of DSP.

On account of two sets of three-phase windings of the DTP PMSM physically independent of each other, the motor can operate in STP mode, which is very necessary for the oil pump safety. Particularly, in case of one set of windings broken down, the other set of windings can continue working to reduce mechanical impact and protect equipment. In addition, when the load is small requiring lower driving power, the DTP PMSM can be switched to STP operation mode driven by one set of three-phase windings, so as to reduce the switching times of IGBTs and the energy loss of the controller.

VI. EXPERIMENTAL VERIFICATION AND DISCUSSIONS

A prototype of the DTP PMSM and the controller was fabricated according to the design scheme, and several experiments were carried out on the experimental setup as shown in Fig. 12. The test DTP PMSM was under the control pattern of rotational speed driven by the DTP PMSM controller. The induction motor working in torque mode could change the load torque of the DTP PMSM.

A. VALIDATION OF STEADY-STATE PERFORMANCE

In order to evaluate the steady-state performance of the motor, the back EMF and current waveforms of the motor at 3000 rpm with no load and rated load were recorded and presented in Figs. 13 (a)-(c).

Fig. 13 (a) shows the line back EMF of the designed DTP PMSM at the rated speed. Intuitively, the voltage waveform is sinusoidal and has less harmonics. The P-P (peak to peak)

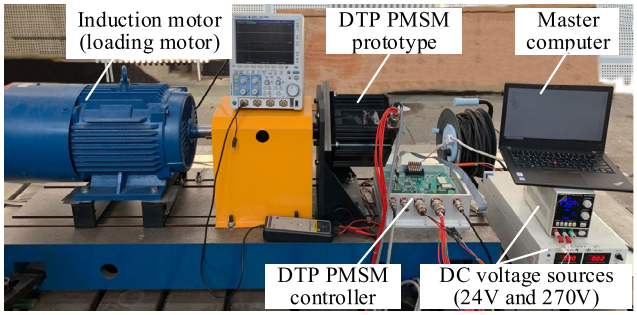

FIGURE 12. **Photograph of the experimental setup.**

value of the line voltage is 519 V and the RMS is 175 V, which are very close to the electromagnetic analysis results in Fig. 7. The reason for the difference between experiment and simulation results is that the actual parameters of the permanent magnet will change due to the influence of the environment temperature.

We compared the steady-state performance of the two control algorithms, ACR based on the dual *d-q* model and VSD, under rated conditions (3000 rpm, 19.1 Nm). The stator current waveform and FFT results are shown in Figs. 13 (b)-(c). For the results based on the dual *d-q* control, the RMS of phase A current (i_A) is 13.01 A and that of phase *X* (i_X) is 12.38A. As for the VSD control, the RMS of i_A is 11.73 A and that of i_X is 13.67 A. The experimental results of steady-state current are consistent with the simulation results (RMS 11.5A) obtained by electromagnetic analysis, but the test bench has large mechanical moment of inertia and friction resistance, hence, the larger current is needed to reach the rated torque. Through FFT analysis, the 1st to 12th order current are illustrated, and as can be seen in Figs. 13 (b)-(c), the harmonic components are mainly 5th and 7th order accounting for a small proportion. In addition, the current THD for VSD control strategy (under 8.0%) is lower than that for dual *d-q* control strategy (over 9.0%). It can be seen from Fig.10(c) that the harmonic current references (i_{z1}^*, i_{z2}^*) are set to zero based on decoupled model, while the dual *d-q* control in Fig.10(b) do not suppress harmonic components because of the coupled currents. Thus, VSD control strategy can reduce current harmonics which is consistent with the experimental results. It should be noted that THD of practical current will never be zero due to the existence of inverter delay and measurement errors.

To further compare the effect of the control algorithms on the DTP PMSM system efficiency, a series of loading tests at the rated speed were performed. A DC power supply provides the input DC power to the inverter, and the voltage (U_{DC}) as well as the current (I_{DC}) is measured. According to the experimental results, the overall efficiency of the proposed DTP PMSM system (η) is obtained by (12):

$$\eta = \frac{P_{out}}{P_{in}} = \frac{T_L n}{9549 U_{DC} I_{DC}} \tag{12}$$

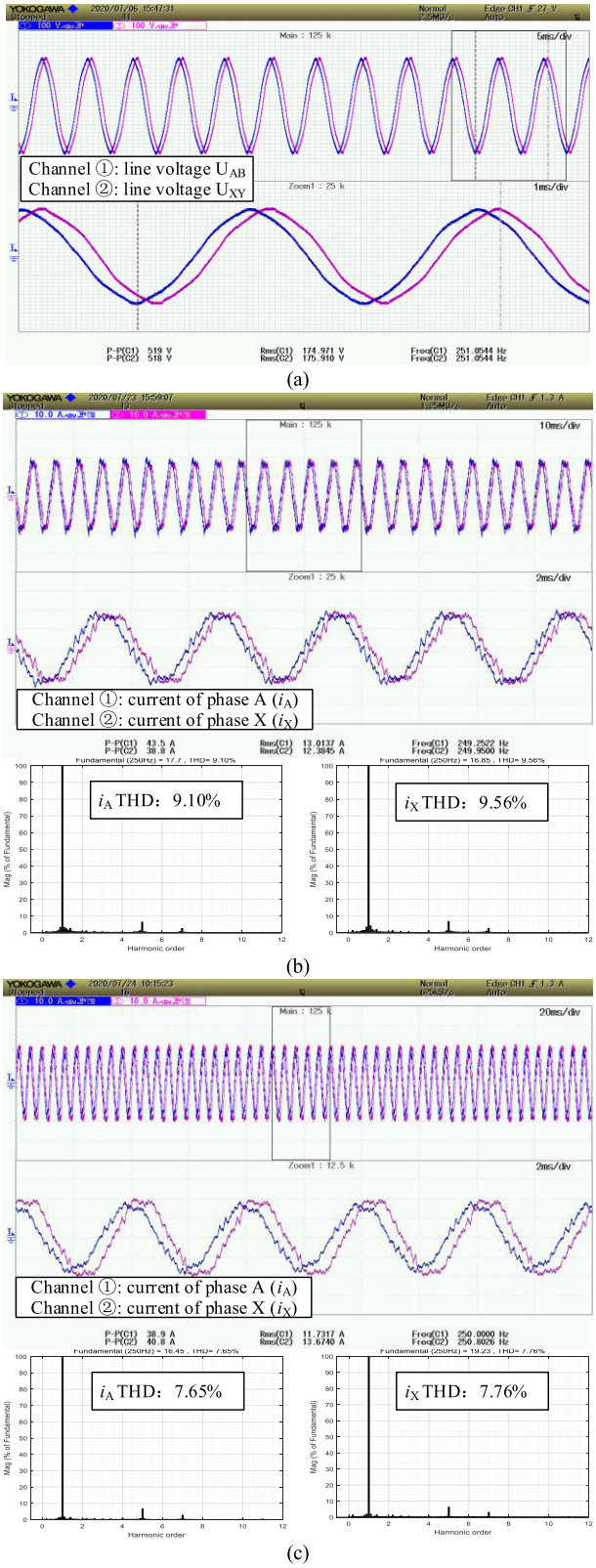

FIGURE 13. **Experimental results at steady states with no load and rated load. (a) Stator line back EMF voltage waveform of the DTP PMSM with no load at 3000 rpm. (b) Stator current waveform and FFT under the rated load at 3000 rpm for dual *d-q* control strategy. (c) Stator current waveform and FFT under the rated load at 3000 rpm for VSD control strategy.**

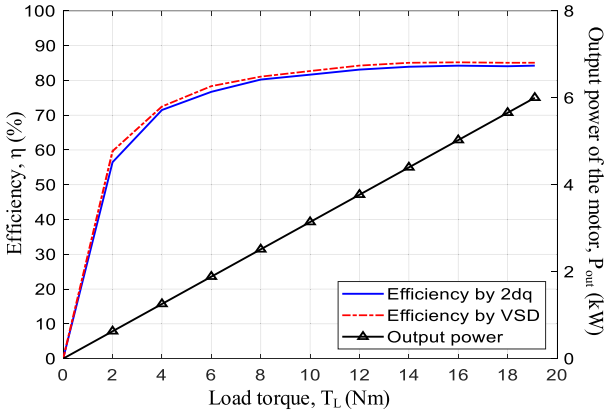

FIGURE 14. Efficiency and power curves of the DTP PMSM system with different control algorithms at 3000 rpm.

where P_{out} is the mechanical output power of the motor, P_{in} is the input electrical power, and T_L and n are the load torque (Nm) and speed (rpm) of the motor respectively. The efficiency and power curves are shown in Fig. 14. At a higher load torque up to the power limit (6 kW), the output power increases and so does the efficiency. The efficiency of the motor implemented with the VSD algorithm is higher than that with dual *d-q* algorithm, and the maximum efficiency is about 85% achieved at the rated load. Compared with dual *d-q* algorithm, because of lower current harmonics leading to less harmonic loss [18], the VSD algorithm can increase the fundamental current promoting the efficiency under the same load. In summary, VSD algorithm is superior to the other one for the motor steady-state control to reduce system power loss.

B. PERFORMANCE IN OPERATION MODE SWITCHING

An experiment for switching operation mode was devised to measure the fault-tolerant performance of the motor system. In the experiment, a switching step signal was injected into the algorithm to cut off the voltage output of phase *XYZ* of the controller to simulate phase failure. The controller was able to automatically switch from DTP mode to STP mode after the failure. With a view to the reduction of maximum torque in STP mode, we selected a typical working condition (2000 rpm, 10 Nm) instead of the rated condition to prevent the motor from over current.

Fig. 15 (a) shows the stator current waveforms during switching as well as the fluctuation of the speed and torque. From the phase current point of view, i_X goes to zero after switching, but the other set of windings (*ABC*) is unable to provide enough torque immediately to balance with the load, so the speed drops rapidly. After the speed decreasing, the ASR adjusts the current reference rapidly to increase the electromagnetic torque of the motor to exceed the load torque, and the motor starts to accelerate. When the speed returns to the target, i_A is reduced and the electromagnetic torque is decreased as well to reach the load torque. In the process,

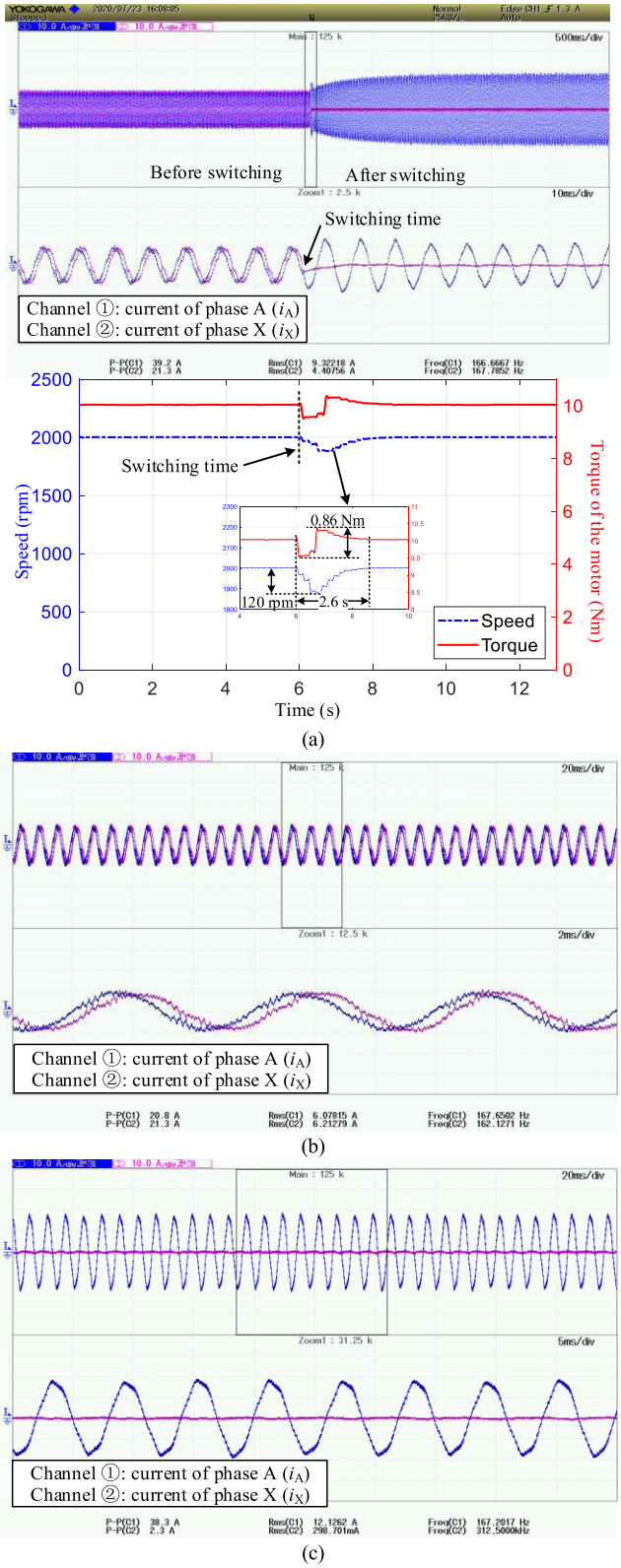

FIGURE 15. Current of phase *A* and phase *X* before/after switching from DTP mode to STP mode under typical operating conditions (2000 rpm, 10 Nm). (a) Current, torque and speed of the motor during switching. (b) Current under DTP mode. (c) Current under STP mode (only ABC phase windings are working, $i_X = 0$).

the motor speed is in a 6% fluctuation (120 rpm) and the torque is in an 8.6% fluctuation (0.86 Nm). And it takes 2.6 seconds for the controller to track the speed reference under the given load torque, which show a good performance.

Before switching, i_A and i_X are about 6.0 A (RMS) in the steady state as the controller is operating in DTP mode as shown in Fig. 15 (b). After switching to STP mode, the steady-state value of i_A increases to 12.1 A that is twice as large as before as seen in Fig.15 (c). It can be seen that, the winding fault affects the phase current significantly, since the electromagnetic torque of the DTP PMSM is generated by two sets of windings according to (4). Assuming that the current RMS value of the two sets of windings is completely equal, then $i_{q1} = i_{q2}$, $i_{d1} = i_{d2} = 0$. And the current of STP mode will be doubled so that it can achieve the same T_e as that of DTP mode. Therefore, in the process of the fault-tolerant control strategy design, the phase current must be reasonably restricted to avoid over-current fault.

VII. CONCLUSION

In this article, a 6kW DTP PMSM system has been developed for driving auxiliary systems in eTransportation application. Digital collaborative develop process was proposed with the support of multiple software tools. The DTP PMSM, the six-phase two-level inverter and the control algorithm were synergistically designed and iteratively optimized. Complete development details including motor scheme optimizing, electromagnetic analysis, modeling and control design of the system were reported. The prototype testing and experimental results indicate that the 6kW DTP PMSM system is qualified for the actual application requirements, and the proposed development process has practical value in engineering.

Since the control strategy using the VSD algorithm in steady-state control and the dual d-q control algorithm in fault tolerance can improve the performance with both superior steady-state control and fault tolerance, a robust switching algorithm realizing smooth excessive will be studied in our future work. DTP PMSMs are gaining wide attention in the field of electrified transportation. This article makes some preliminary attempts in their high-efficiency development, and more practical work aiming at eTransportation demands will be launched in the future.

REFERENCES

[1] J. Du and M. Ouyang, "Review of electric vehicle technologies progress and development prospect in China," in *Proc. World Electric Vehicle Symp. Exhib. (EVS)*, Nov. 2013, pp. 1–8.

[2] Z. Shuai, H. Zhang, J. Wang, J. Li, and M. Ouyang, "Combined AFS and DYC control of four-wheel-independent-drive electric vehicles over CAN network with time-varying delays," *IEEE Trans. Veh. Technol.*, vol. 63, no. 2, pp. 591–602, Feb. 2014.

[3] A. Emadi, "Transportation 2.0," *IEEE Power Energy Mag.*, vol. 9, no. 4, pp. 18–29, Jul./Aug. 2011.

[4] R. Bojoi, S. Rubino, A. Tenconi, and S. Vaschetto, "Multiphase electrical machines and drives: A viable solution for energy generation and transportation electrification," in *Proc. Int. Conf. Expo. Electr. Power Eng. (EPE)*, Oct. 2016, pp. 632–639.

[5] E. Levi, "Multiphase electric machines for variable-speed applications," *IEEE Trans. Ind. Electron.*, vol. 55, no. 5, pp. 1893–1909, May 2008.

[6] R. Bojoi, A. Cavagnino, A. Tenconi, A. Tessarolo, and S. Vaschetto, "Multiphase electrical machines and drives in the transportation electrification," in *Proc. IEEE 1st Int. Forum Res. Technol. Soc. Ind. Leveraging Better Tomorrow (RTSI)*, Sep. 2015, pp. 205–212.

[7] R. Yang, N. Schofield, N. Zhao, and A. Emadi, "Dual three-phase permanent magnet synchronous machine investigation for battery electric vehicle power-trains," *J. Eng.*, vol. 2019, no. 17, pp. 3981–3985, Jun. 2019.

[8] S. Hu, Z. Liang, W. Zhang, and X. He, "Research on the integration of hybrid energy storage system and dual three-phase PMSM drive in EV," *IEEE Trans. Ind. Electron.*, vol. 65, no. 8, pp. 6602–6611, Aug. 2018.

[9] F. de Luca, V. Calderaro, V. Galdi, and A. Piccolo, "A fuzzy control for a nine-phase integrated on-board battery charger," in *Proc. IEEE PES Innov. Smart Grid Technol. Eur. (ISGT-Eur.)*, Sep. 2019, pp. 1–5.

[10] A. Sivert, F. Betin, M. Moghadasian, A. Yazidi, and G. A. Capolino, "Position control of six-phase induction motor using fuzzy logic: Application to electric power steering," in *Proc. 20th Int. Conf. Elect. Mach.*, Sep. 2012, pp. 1055–1061.

[11] A. Matyas, G. Aroquiadassou, C. Martis, A. Mpanda-Mabwe, and K. Biro, "Design of six-phase synchronous and induction machines for EPS," in *Proc. 19th Int. Conf. Electr. Mach. (ICEM)*, Sep. 2010, pp. 1–6.

[12] K. Y. Hwang, B. K. Song, and B. I. Kwon, "Asymmetric dual winding three-phase PMSM for fault tolerance of overheat in electric braking system of autonomous vehicle," *IET Electr. Power Appl.*, vol. 13, no. 12, pp. 1891–1898, 2019.

[13] M. Barcaro, N. Bianchi, and F. Magnussen, "Six-phase supply feasibility using a PM fractional-slot dual winding machine," *IEEE Trans. Ind. Appl.*, vol. 47, no. 5, pp. 2042–2050, Sep. 2011.

[14] K. Wang and H. Lin, "A novel 24-slot/10-pole dual three-phase fractional-slot overlapped winding for low non-working space harmonics and stator modularization," *IEEE Access*, vol. 8, pp. 85490–85503, 2020.

[15] S. Zhu, W. Zhao, G. Liu, Y. Mao, and Y. Sun, "Effect of phase shift angle on radial force and vibration behavior in dual three-phase PMSM," *IEEE Trans. Ind. Electron.*, early access, Mar. 6, 2020, doi: 10.1109/TIE.2020.2977578.

[16] H. Kim, K. Shin, S. Englebretson, N. Frank, and W. Arshad, "Analytical model of multiphase permanent magnet synchronous machines for energy and transportation applications," in *Proc. Int. Electr. Mach. Drives Conf.*, May 2013, pp. 172–179.

[17] J. Sabarad, G. H. Kulkarni, and S. Sattigeri, "Dual three phase induction motor control using five leg inverter," in *Proc. Int. Conf. Smart Grids, Power Adv. Control Eng. (ICSPACE)*, Aug. 2017, pp. 120–125.

[18] Y. Xu, B. Zheng, G. Wang, H. Yan, and J. Zou, "Current harmonic suppression in dual three-phase permanent magnet synchronous machine with extended state observer," *IEEE Trans. Power Electron.*, vol. 35, no. 11, pp. 12166–12180, Nov. 2020.

[19] S. Liu and C. Liu, "Virtual-vector based robust predictive current control for dual three-phase PMSM," *IEEE Trans. Ind. Electron.*, early access, Feb. 20, 2020, doi: 10.1109/TIE.2020.2973905.

[20] Z. Liang, D. Liang, P. Kou, and S. Jia, "Postfault control and harmonic current suppression for a symmetrical dual three-phase SPMSM drive under single-phase open-circuit fault," *IEEE Access*, vol. 8, pp. 67674–67686, 2020.

[21] L. Xiao, L. Zhang, F. Gao, and J. Qian, "Robust fault-tolerant synergetic control for dual three-phase PMSM drives considering speed sensor fault," *IEEE Access*, vol. 8, pp. 78912–78922, 2020.

[22] L. Zhang, Y. Fan, C. Li, and C. Liu, "Design and analysis of a new six-phase fault-tolerant hybrid-excitation motor for electric vehicles," *IEEE Trans. Magn.*, vol. 51, no. 11, pp. 1–4, Nov. 2015.

[23] F. Jin, J. Si, Z. Cheng, P. Su, L. Dong, and G. Qi, "Analysis of a six-phase direct-drive permanent magnet synchronous motor with novel toroidal windings," in *Proc. IEEE Vehicle Power Propuls. Conf. (VPPC)*, Oct. 2019, pp. 1–6.

[24] K. K. Mohapatra, R. S. Kanchan, M. R. Baiju, P. N. Tekwani, and K. Gopakumar, "Independent field-oriented control of two split-phase induction motors from a single six-phase inverter," *IEEE Trans. Ind. Electron.*, vol. 52, no. 5, pp. 1372–1382, Oct. 2005.

[25] Y. Xu, H. Yan, and J. Zou, "A fault-tolerant control strategy for six-phase transverse flux tubular PMLM based on synthetic vector method," *IEEE Trans. Plasma Sci.*, vol. 43, no. 5, pp. 1332–1338, May 2015.

[26] H. Dhulipati, E. Ghosh, S. Mukundan, P. Korta, J. Tjong, and N. C. Kar, "Advanced design optimization technique for torque profile improvement in six-phase PMSM using supervised machine learning for direct-drive EV," *IEEE Trans. Energy Convers.*, vol. 34, no. 4, pp. 2041–2051, Dec. 2019.

[27] K. K. Nallamekala and K. Sivakumar, "A fault-tolerant dual three-level inverter configuration for multipole induction motor drive with reduced torque ripple," *IEEE Trans. Ind. Electron.*, vol. 63, no. 3, pp. 1450–1457, Mar. 2016.
[28] Y. Kim, J. Lee, C. Jo, Y. Kim, M. Song, J. Kim, and H. Kim, "Development and control of an electric oil pump for automatic transmission-based hybrid electric vehicle," *IEEE Trans. Veh. Technol.*, vol. 60, no. 5, pp. 1981–1990, 2011.
[29] J. Wi, H. Kim, J. Yoo, H. Son, H. Kim, and B. Kim, "Energy consumption of parallel type hybrid electric vehicle with continuously variable transmission using electric oil pump," in *Proc. 13th Int. Conf. Ecological Vehicles Renew. Energies (EVER)*, Apr. 2018, pp. 1–7.
[30] C. Fimmers, S. Wein, S. Storms, C. Brecher, T. Deppe, U. Epple, and O. Graeser, "An industry 4.0 engineering workflow approach: From product catalogs to product instances," in *Proc. 45th Annu. Conf. IEEE Ind. Electron. Soc. (IECON)*, Oct. 2019, pp. 2922–2927.
[31] A. Kempitiya and W. Chou, "An electro-thermal performance analysis of SiC MOSFET vs Si IGBT and diode automotive traction inverters under various drive cycles," in *Proc. 34th Thermal Meas., Modeling Manage. Symp. (SEMI-THERM)*, Mar. 2018, pp. 213–217.
[32] D. Athaide, J. Qin, and Y. Zou, "MATLAB/Simulink-based electromagnetic transient-transient stability hybrid simulation for electric power systems with converter interfaced generation," in *Proc. IEEE Texas Power Energy Conf. (TPEC)*, Feb. 2019, pp. 1–6.
[33] W. Xiaojie, D. Peng, and Z. Dongsheng, "Full digital control and application of high power synchronous motor drive with dual stator winding fed by cycloconverter," in *Proc. 5th Int. Conf. Power Electron. Drive Syst. (PEDS)*, Nov.2003, pp. 1194–1199.
[34] Y. Zhao and T. A. Lipo, "Space vector PWM control of dual three-phase induction machine using vector space decomposition," *IEEE Trans. Ind. Appl.*, vol. 31, no. 5, pp. 1100–1109, 1995.

SHUAI HE received the B.E. degree in automotive engineering from Tsinghua University, Beijing, China, in 2018. He is currently pursuing the M.E. degree with the China North Vehicle Research Institute, Beijing. His main research interests include motor control and embedded systems.

YAOHENG LI received the B.E. degree in electrical engineering and automation from Shijiazhuang Tiedao University, Hebei, China, in 2013, and the M.E. degree in electrical engineering from Beijing Jiaotong University, Beijing, China, in 2016.

Since 2016, he has been an Engineer with the Science and Technology on Vehicle Transmission Laboratory, China North Vehicle Research Institute, Beijing. His research interests include power electronics and AC drives.

GUANGMING ZHOU received the B.E. degree in vehicle engineering from the Beijing Institute of Technology, Beijing, China, in 1986.

He joined the China North Vehicle Research Institute, Beijing, in 1986, as an Engineer, where he has been engaged in the researching work on vehicle transmission system for a long time. Since 1996, he has been a Researcher with the Science and Technology on Vehicle Transmission Laboratory, China North Vehicle Research Institute. His current research interests include control, and advanced technology for energy and materials.

Mr. Zhou was a recipient of the State Science and Technology Awards of China twice.

JIANGTAO GAI received the B.E. and M.E. degrees in vehicle engineering from the Beijing Institute of Technology, Beijing, China, in 2004 and 2006, respectively, and the Ph.D. degree in electrical engineering from Hunan University, Hunan, China, in 2015.

Since 2016, he has been a Researcher with the Science and Technology on Vehicle Transmission Laboratory, China North Vehicle Research Institute, Beijing. He has participated in a lot of research work for automotive electric drive supported by the National Science Foundation of China as the Key Researcher. His main research interests include power electronics and electrical drives.

YASHAN HU received the B.E. and M.S. degrees from Northwestern Polytechnical University, Xi'an, China, in 2002 and 2005, respectively, and the Ph.D. degree from the University of Sheffield, Sheffield, U.K., in 2016, all in electronic and electrical engineering.

From 2016 to 2018, he was with Siemens Wind Power A/S, Denmark, as an Advanced Research Engineer. Since 2018, he has been an Associate Professor with the College of Electrical and Information Engineering, Hunan University. His current research interests include electrical machine control and drives for wind energy conversion systems.

YONG LI received the Ph.D. degree in electrical engineering from Beijing Jiaotong University, Beijing, China, in 2019.

He is currently a Senior Engineer with the Science and Technology on Vehicle Transmission Laboratory, China North Vehicle Research Institute, Beijing. He has been engaged in theoretical research and structural design of PMSMs, large-scale turbine synchronous generator, and researching on comprehensive physical field of electromagnetic loss and heat exchange in the motor for many years. His research interests include motor design and electromagnetic analysis.

YING ZHANG received the B.E. degree in automation from the Hefei University of Technology, Anhui, China, in 2016, and the M.E. degree in control engineering from Beihang University, Beijing, China, in 2019.

Since 2019, she has been an Engineer with the Science and Technology on Vehicle Transmission Laboratory, China North Vehicle Research Institute, Beijing. Her research interests include motor control and electrical systems.

YAO CHEN received the B.E. degree from the Wuhan University of Science and Technology, Wuhan, China, in 2017, and the M.S. degree from the China North Vehicle Research Institute, Beijing, China, in 2020, all in vehicle engineering.

He is currently an Assistant Engineer with the Science and Technology on Vehicle Transmission Laboratory, China North Vehicle Research Institute. His research interests include thermal analysis and motor control.

DERONG LUO was born in Hunan, China, in 1968. He received the M.S. and Ph.D. degrees from the College of Electrical and Information Engineering, Hunan University, Changsha, China, in 1990 and 2003, respectively. He is currently a Professor with the College of Electrical and Information Engineering, Hunan University. His research interests include permanent magnet synchronous motor drives, and position sensorless control of AC motors.

YAOJING FENG was born in Hunan, China, in 1985. She received the Ph.D. degree in electrical engineering from the Huazhong University of Science and Technology, Wuhan, China, in 2012.

She is currently an Associate Professor of electrical engineering with the College of Electrical and Information Engineering, Hunan University, Changsha, China. Her main research interests include permanent magnet machines, design and control of electrical motors, and electric vehicle (EV) drive systems.

ZHIBIN SHUAI (Member, IEEE) received the B.E. degree in automotive engineering and the Ph.D. degree in power machine and engineering from Tsinghua University, Beijing, China, in 2009 and 2015, respectively.

From August 2012 to September 2013, he was a Visiting Ph.D. Student with the Vehicle Systems and Control Laboratory, Department of Mechanical and Aerospace Engineering, The Ohio State University, Columbus, OH, USA. He is currently an Associate Researcher with the China North Vehicle Research Institute, Beijing. His research interests include embedded systems, vehicle dynamics and control, tracked and wheeled vehicles, electrified transportation, motor control, and power electronics.